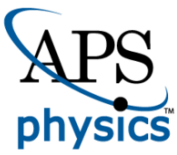

Enhancing photovoltaic power by Fano-induced coherence

Anatoly A. Svidzinsky, Konstantin E. Dorfman, and Marlan O. Scully

Phys. Rev. A **84**, 053818 — Published 10 November 2011

DOI: 10.1103/PhysRevA.84.053818

Enhancing photovoltaic power by Fano induced coherence

Anatoly A. Svidzinsky, Konstantin E. Dorfman and Marlan O. Scully
Texas A&M University, College Station TX 77843 and Princeton University, Princeton NJ 08544

We show that coherence induced by Fano interference can enhance power generated by a photovoltaic device as compared to the same system with no coherence. No additional external energy source is necessary to create such induced coherence. In the present model, coherence increases the flow of electrons through the load which reduces radiative recombination and enhances cell power.

PACS numbers: 84.60.Jt, 64.10.+h

It has been demonstrated that quantum coherence yields interesting phenomena such as lasing without inversion [1] and quantum heat engines which can extract useful work from a single thermal reservoir without violating the second law of thermodynamics [2].

Recently it has been shown [3] that it is possible to use radiatively induced quantum coherence to break detailed balance and enhance the quantum efficiency (i.e. open circuit voltage) of a quantum dot photocell depicted in Fig. 1b. There the external drive field (which induces coherence between levels a_1 and a_2) serves as an additional energy source which yields enhancement of the voltage [4]. However, as noted in [3]: "It is possible to generate coherence without the use of an external field. For example, quantum noise induced coherence via Fano coupling yields enhanced cell efficiency" [5].

The toy quantum dot photocell model of [3] is concerned with issues of principal rather than practical implications. A. Kirk [6] attempts to investigate the limits of Ref. [3] and, in particular, argues that Fano interference does not break detailed balance [7]. Here we show, however, that coherence produced by Fano interference does indeed enhance the balance breaking and can yield an increase of the cell power. Namely, we demonstrate that the power delivered to the load can be enhanced by Fano coupling, as depicted in Fig. 2. Our findings are along the lines of S. Harris work [8] which shows that Fano interference can result in suppression of absorption via breaking of detailed balance and laser amplification without population inversion [9]. However, in the present scheme, Fano interference produces the opposite effect and reduces undesired photon emission.

Next we present a brief account of Agarwal-Fano coupling [10] for a simple problem of radiative decay of $|a_1\rangle$ and $|a_2\rangle$ levels into the ground state $|b\rangle$ with the emission of a photon of wave vector $\mathbf{k}$. The state vector for the system reads

$$|\psi\rangle = \alpha_1(t)|a_1,0\rangle + \alpha_2(t)|a_2,0\rangle + \sum_{\mathbf{k}} \beta_{\mathbf{k}}(t)|b,1_{\mathbf{k}}\rangle, \quad (1)$$

where $|0\rangle$ and $|1_{\mathbf{k}}\rangle$ are the vacuum and single photon states respectively. For the probability amplitudes α_1, α_2 and $\beta_{\mathbf{k}}$ the Schrödinger equation yields

$$\dot\alpha_1(t) = -i\sum_{\mathbf{k}} g^*_{1\mathbf{k}}\beta_{\mathbf{k}} e^{i(\omega_{1b}-\nu_{\mathbf{k}})t}, \quad (2)$$

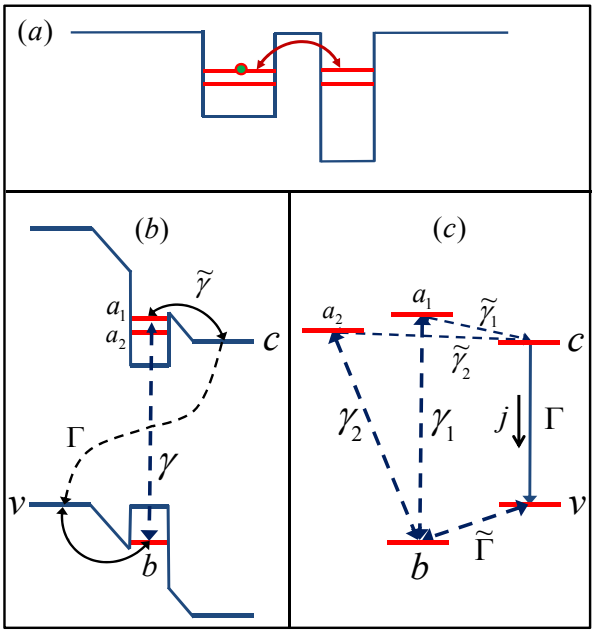

FIG. 1: (Color online) (*a*) Splitting of quantum dot degenerate levels by electron tunneling between adjacent dots. (b) Quantum dot photocell with Fano doublet $|a_1\rangle$, $|a_2\rangle$ coupled to conduction $|c\rangle$ and valence $|v\rangle$ reservoir states in the right and left sides of photocell pn junction. (c) Corresponding energy level diagram of the cell model. Solar radiation drives transitions between the ground state $|b\rangle$ and the two upper levels. Other transitions are driven by ambient thermal phonons. Levels c and v are connected to a load.

$$\dot\alpha_2(t) = -i\sum_{\mathbf{k}} g^*_{2\mathbf{k}}\beta_{\mathbf{k}} e^{i(\omega_{2b}-\nu_{\mathbf{k}})t}, \quad (3)$$

$$\dot\beta_{\mathbf{k}}(t) = -ig_{1\mathbf{k}}\alpha_1 e^{-i(\omega_{1b}-\nu_{\mathbf{k}})t} - ig_{2\mathbf{k}}\alpha_2 e^{-i(\omega_{2b}-\nu_{\mathbf{k}})t}, \quad (4)$$

where $g_{i\mathbf{k}}$ $(i = 1,2)$ is the coupling constant for the $|a_i,0\rangle \to |b,1_{\mathbf{k}}\rangle$ transition, $\hbar\omega_{ib} = E_{a_i} - E_b$ is the energy spacing between levels $|a_i\rangle$ and $|b\rangle$, $\nu_{\mathbf{k}}$ is the photon frequency. We proceed by integrating Eq. (4) and substituting the result into Eqs. (2) and (3). Following the

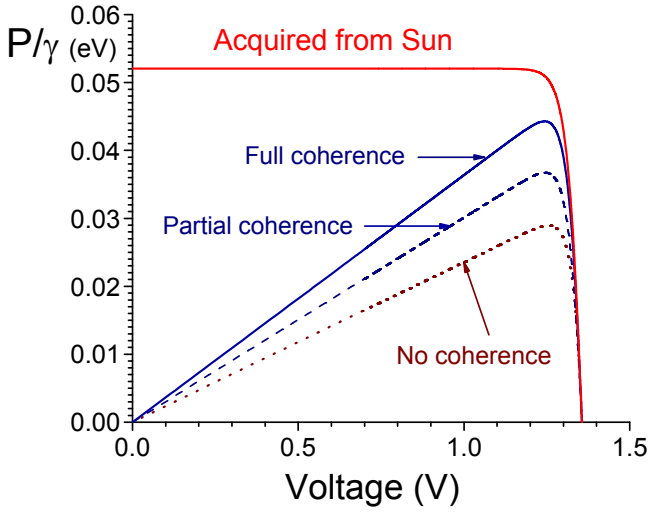

FIG. 2: (Color online) Power generated by a photovoltaic cell P as a function of induced cell voltage V with and without Fano interference. Solid line is calculated for $\gamma_{12} = \sqrt{\gamma_1\gamma_2}$ and $\tilde{\gamma}_{12} = \sqrt{\tilde{\gamma}_1\tilde{\gamma}_2}$ (full coherence), dash line corresponds to $\gamma_{12} = 0$ and $\tilde{\gamma}_{12} = \sqrt{\tilde{\gamma}_1\tilde{\gamma}_2}$ (partial coherence), while for dot curve $\gamma_{12} = \tilde{\gamma}_{12} = 0$ (no coherence). Upper curve indicates power acquired from the sun $P_S = j \cdot E_{ab}/e$.

Weisskopf-Wigner approach [11] we find

$$\dot{\alpha}_1 = -\frac{\gamma_1}{2}\alpha_1 - \frac{\sqrt{\gamma_1\gamma_2}}{2}\alpha_2, \quad \dot{\alpha}_2 = -\frac{\gamma_2}{2}\alpha_2 - \frac{\sqrt{\gamma_1\gamma_2}}{2}\alpha_1, \tag{5}$$

where γ_i is the radiative decay rate of the level $|a_i\rangle$. The expressions (5) apply to the simple case of $\omega_{1b} = \omega_{2b}$ and real matrix elements ($g_{i\mathbf{k}} = g^*_{i\mathbf{k}}$). Physically the Agarwal-Fano coupling terms, $\sqrt{\gamma_1\gamma_2}$, are the result of virtual emission and reabsorption of radiation such as $|a_1, 0\rangle \to |b, 1_{\mathbf{k}}\rangle \to |a_2, 0\rangle$ etc.

In the following we consider the more general Fano coupling associated with emission and absorption of solar photons and thermal phonons. This will require a more detailed density matrix analysis but the physics is essentially the same. Furthermore, we here focus on the power generated, not the open circuit voltage as in [3]. However, the issue of breaking detailed balance in a photocell remains the essence of the problem here as well.

Proceeding with the analysis, we consider (as in [3]) a photovoltaic cell model with an array of 3-level quantum dots [12] with two levels $|a_1\rangle$ and $|a_2\rangle$ in the conduction band and level $|b\rangle$ in the valence band (see Fig. 1c). Doublet $|a_1\rangle$ and $|a_2\rangle$ can be produced, e.g., by splitting of degenerate quantum dot levels due to electron tunneling between adjacent dots (see Fig. 1a). The electronic system interacts with radiation and phonon thermal reservoirs. We assume that thermal solar photons with frequency midway between ω_{1b} and ω_{2b} are directed onto the cell. They drive $b \leftrightarrow a_1$ and $b \leftrightarrow a_2$ transitions and have average occupation number $n = \left[\exp\left(\frac{E_{ab}}{k_B T_S}\right) - 1\right]^{-1}$, where $E_{ab} = (E_{1b} + E_{2b})/2$. Ambient thermal phonons at temperature T_a drive the low energy transitions $c \leftrightarrow a_1$, $c \leftrightarrow a_2$ and $b \leftrightarrow v$. The corresponding phonon occupation numbers are $n_c = \left[\exp\left(\frac{E_{ac}}{k_B T_a}\right) - 1\right]^{-1}$ and $n_v = \left[\exp\left(\frac{E_{vb}}{k_B T_a}\right) - 1\right]^{-1}$, where $E_{ac} = (E_{1c} + E_{2c})/2$. We also assume that level c and level v are connected to a load (e.g. resistor), and level v decays into the ground state b at a rate $\tilde{\Gamma}$ (see Fig. 1c). We model the load as yielding a decay of the level c into level v at a rate Γ.

In the Weisskopf-Wigner approximation we obtain the following equations for the density matrix ($\rho_{a_i a_k} \equiv \rho_{ik}$) [13]

$$\dot{\rho}_{11} = -\gamma_1\left[(n+1)\rho_{11} - n\rho_{bb}\right] - \tilde{\gamma}_1\left[(n_c+1)\rho_{11} - n_c\rho_{cc}\right]$$

$$-\gamma_{12}(n+1)\mathrm{Re}[\rho_{12}] - \tilde{\gamma}_{12}(n_c+1)\mathrm{Re}[\rho_{12}], \tag{6}$$

$$\dot{\rho}_{22} = -\gamma_2\left[(n+1)\rho_{22} - n\rho_{bb}\right] - \tilde{\gamma}_2\left[(n_c+1)\rho_{22} - n_c\rho_{cc}\right]$$

$$-\gamma_{12}(n+1)\mathrm{Re}[\rho_{12}] - \tilde{\gamma}_{12}(n_c+1)\mathrm{Re}[\rho_{12}], \tag{7}$$

$$\dot{\rho}_{12} = -\left(i\Delta + \frac{1}{2}\left[(\gamma_1+\gamma_2)(n+1) + (\tilde{\gamma}_1+\tilde{\gamma}_2)(n_c+1)\right]\right)\rho_{12}$$

$$-\frac{\gamma_{12}}{2}\left[(n+1)\rho_{22} + (n+1)\rho_{11} - 2n\rho_{bb}\right]$$

$$-\frac{\tilde{\gamma}_{12}}{2}\left[(n_c+1)\rho_{22} + (n_c+1)\rho_{11} - 2n_c\rho_{cc}\right] - \frac{\rho_{12}}{\tau_2}, \tag{8}$$

$$\dot{\rho}_{cc} = \tilde{\gamma}_1\left[(n_c+1)\rho_{11} - n_c\rho_{cc}\right] + \tilde{\gamma}_2\left[(n_c+1)\rho_{22} - n_c\rho_{cc}\right]$$

$$+2\tilde{\gamma}_{12}(n_c+1)\mathrm{Re}[\rho_{12}] - \Gamma\rho_{cc}, \tag{9}$$

$$\dot{\rho}_{vv} = \Gamma\rho_{cc} - \tilde{\Gamma}(n_v+1)\rho_{vv} + \tilde{\Gamma}n_v\rho_{bb}, \tag{10}$$

$$\rho_{bb} = 1 - \rho_{11} - \rho_{22} - \rho_{cc} - \rho_{vv}, \tag{11}$$

where γ_i and $\tilde{\gamma}_i$ are spontaneous decay rates of the corresponding transitions (see Fig. 1c), τ_2 is the decoherence time, and $\Delta = \omega_{1b} - \omega_{2b}$ is the splitting of the levels a_1 and a_2. For maximum Fano coherence $\gamma_{12} = \sqrt{\gamma_1\gamma_2}$ and $\tilde{\gamma}_{12} = \sqrt{\tilde{\gamma}_1\tilde{\gamma}_2}$, while for no interference $\gamma_{12} = \tilde{\gamma}_{12} = 0$.

We focus on steady state operation. In this regime one can solve Eqs. (6)-(11) and obtain level populations and coherence ρ_{12}. In particular, if levels a_1 and a_2 are degenerate and $\gamma_1 = \gamma_2 = \gamma$, $\tilde{\gamma}_1 = \tilde{\gamma}_2 = \tilde{\gamma}$ we find that current j through the cell is given by (we neglect decoherence $1/\tau_2$ which can be made small compared to the other coherence decay terms in Eq. (8))

$$j = e\Gamma\rho_{cc} = \frac{2e\gamma(n_c+1)n}{B-A}, \tag{12}$$

where constant B is independent of coherence

$$B = 1 + 2n_v + 2\gamma n \left[\frac{n_v+1}{\Gamma} + \frac{1}{\tilde{\Gamma}}\right]$$

$$+ \left(1 + \frac{2\tilde{\gamma}n_c}{\Gamma}\right) \frac{\gamma\left[(n+1)(1+2n_v) + 2(n_v+1)n\right]}{\tilde{\gamma}(n_c+1)}, \quad (13)$$

while A characterizes the effect of Fano interference (coherence) and depends on γ_{12} and $\tilde{\gamma}_{12}$. For maximum Fano interference ($\gamma_{12} = \gamma$ and $\tilde{\gamma}_{12} = \tilde{\gamma} - \varepsilon$, where ε is a small positive number) we find

$$A = \frac{\gamma n\,(n_v+1)}{\tilde{\gamma}(n_c+1)} \quad \text{and} \quad \rho_{12} = \frac{j}{4e\tilde{\gamma}(n_c+1)}. \quad (14)$$

Eq. (14) shows that nonzero current through the cell j generates coherence ρ_{12}. Fano induced coherence ρ_{12} can result in enhancement of the cell current. For example, for no interference $A = \rho_{12} = 0$ while for maximum interference $A > 0$ (see Eq. (14)) which, according to Eq. (12), yields larger current. Thus, the induced coherence ρ_{12} can increase current through the cell yielding higher efficiency.

In our model, levels c and v are connected to a load. Voltage across the load is expressed in terms of populations of the levels c and v as

$$eV = E_c - E_v + k_B T_a \ln\left(\frac{\rho_{cc}}{\rho_{vv}}\right), \quad (15)$$

where T_a is the ambient temperature. Power delivered to the load is $P = j \cdot V$. To calculate the current-voltage characteristic of the cell we vary Γ at fixed other parameters. $\Gamma = 0$ corresponds to the open circuit. So, by increasing Γ one can go from the open circuit to the short circuit regime.

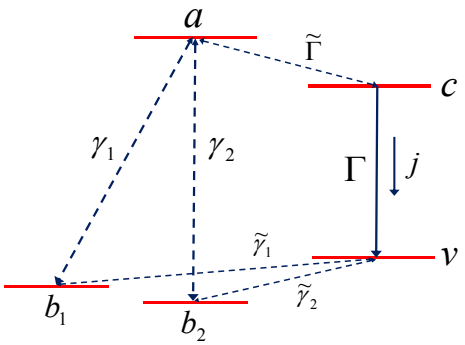

FIG. 3: (Color online) Energy level diagram of the cell model with the lower energy doublet. Solar radiation drives transitions between the upper level a and the two lower levels b_1 and b_2. Other transitions are driven by ambient thermal phonons. Levels c and v are connected to a load.

Next we discuss two limiting cases. For $n_c \simeq n_v \gg 1$, $n \gg 1$, $\Gamma \simeq \gamma$ and $\tilde{\gamma} \ll \tilde{\Gamma} \ll \gamma/n_v$ the current with no coherence is

$$j = \frac{e\tilde{\gamma}n_c}{2}, \quad (16)$$

while for maximum interference it is enhanced by 1/3

$$j = \frac{2e\tilde{\gamma}n_c}{3}. \quad (17)$$

In such a limit, coherence enhances the maximum cell power $P_{\max}$ also by 1/3 so that

$$P_{\max} = \frac{2\tilde{\gamma}n_c}{3}\left[E_{ab}\left(1 - \frac{T_a}{T_S}\right) - k_B T_a \ln\left(\frac{E_{cv}}{k_B T_a}\right)\right]. \quad (18)$$

For $n_c \simeq n_v \ll 1$, $n \gg 1$ and $\tilde{\gamma} \ll \tilde{\Gamma} \ll \gamma \simeq \Gamma$ we obtain that current with no coherence is

$$j = \frac{2e\tilde{\gamma}}{3}, \quad (19)$$

while with coherence j enhances by 50% to

$$j = e\tilde{\gamma}. \quad (20)$$

The maximum cell power is also increased by 50% and given by

$$P_{\max} = \tilde{\gamma}\left[E_{cv} - k_B T_a \ln\left(\frac{E_{cv}}{k_B T_a}\frac{\tilde{\gamma}}{\tilde{\Gamma}}\right)\right]. \quad (21)$$

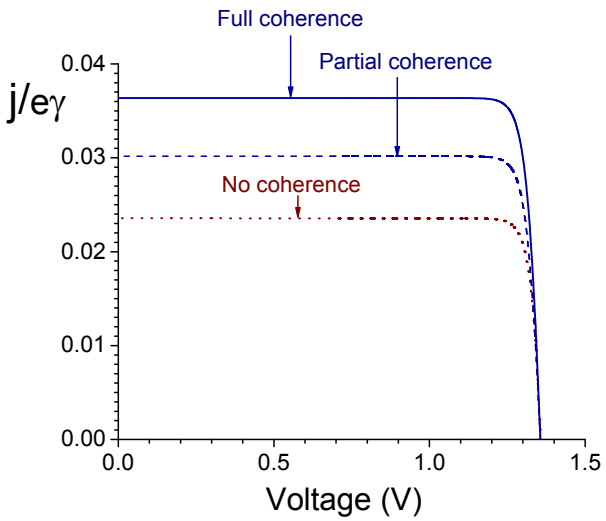

FIG. 4: (Color online) Current-voltage characteristic of a photovoltaic cell with and without Fano interference. Solid line is calculated for $\gamma_{12} = \sqrt{\gamma_1\gamma_2}$ and $\tilde{\gamma}_{12} = \sqrt{\tilde{\gamma}_1\tilde{\gamma}_2}$ (full coherence), dash line corresponds to $\gamma_{12} = 0$ and $\tilde{\gamma}_{12} = \sqrt{\tilde{\gamma}_1\tilde{\gamma}_2}$ (partial coherence), while for dot curve $\gamma_{12} = \tilde{\gamma}_{12} = 0$ (no coherence).

We also note that enhanced power output can be achieved by another possible scheme using Fano interference in which the lower energy level is split into sublevels

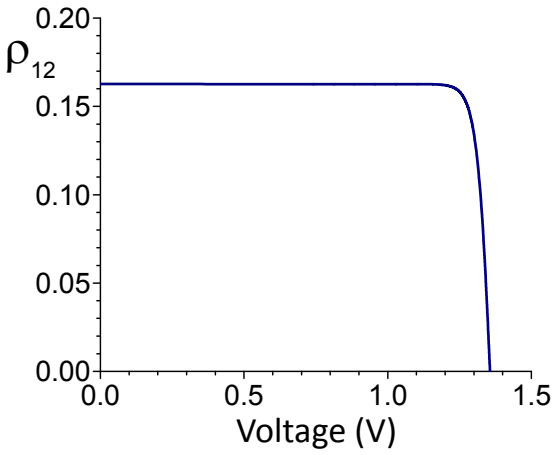

FIG. 5: (Color online) Coherence ρ_{12} between the degenerate levels as a function of the cell voltage for $\gamma_{12} = \sqrt{\gamma_1\gamma_2}$ and $\tilde{\gamma}_{12} = \sqrt{\tilde{\gamma}_1\tilde{\gamma}_2}$. ρ_{12} vanishes if $j = 0$.

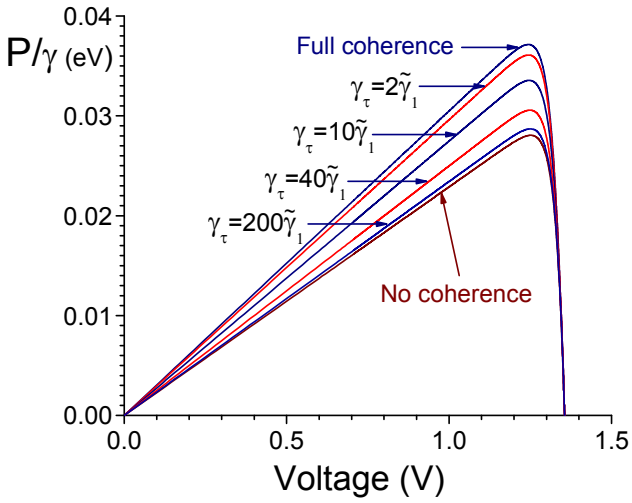

FIG. 6: (Color online) Power of a photocell of Fig. 3 as a function of voltage for different decoherence rates $\gamma_\tau \equiv 1/\tau_2 = 2\tilde{\gamma}_1$, $10\tilde{\gamma}_1$, $40\tilde{\gamma}_1$ and $200\tilde{\gamma}_1$. Here $\tilde{\gamma}_1$ is the fastest spontaneous decay rate in our analysis. The P vs V curves are calculated for the cell parameters given in the text. For these parameters the Fano interference enhances the cell power even if $1/\tau_2$ is much larger than $\tilde{\gamma}_1$.

b_1 and b_2, while there is only one upper level a (see Fig. 3). As an example, in Figs. 2 and 4 we plot the cell power and current as a function of voltage across the load for the photocell of Fig. 3. Coherence $\rho_{b_1b_2} \equiv \rho_{12}$ is plotted in Fig. 5. Solid lines correspond to the case of maximum interference ($\gamma_{12} = \sqrt{\gamma_1\gamma_2}$ and $\tilde{\gamma}_{12} = \sqrt{\tilde{\gamma}_1\tilde{\gamma}_2}$), dash lines indicate the result for $\gamma_{12} = 0$ and $\tilde{\gamma}_{12} = \sqrt{\tilde{\gamma}_1\tilde{\gamma}_2}$ (partial interference), while dot curves are obtained for no coherence ($\gamma_{12} = \tilde{\gamma}_{12} = 0$). In these calculations we assume that levels b_1 and b_2 are degenerate and take $T_S = 0.5$ eV, $T_a = 0.0259$ eV, $E_a - E_b = 1.43$ eV (GaAs band-gap), $E_a - E_c = E_v - E_b = 0.005$ eV, $E_c - E_v = 1.42$ eV, $\gamma_2 = 0.1\gamma_1$, $\tilde{\gamma}_1 = 50\gamma_1$, $\tilde{\gamma}_2 = 5.5\gamma_1$, $\tilde{\Gamma} = 50\gamma_1$ and $1/\tau_2 = 0$. In this example, induced coherence increases the peak power by upto about 50%.

One should note that power supplied by the incident solar radiation $P_S = j \cdot E_{ab}/e$ is always greater then that delivered to the load P. More precisely, $P \leq P_S(1 - T_a/T_S)$, in agreement with the second law of thermodynamics and Rose's work [14] on the resolution of the Shockley paradox.

Finally, we show that for the appropriate cell design, decoherence τ_2 in Eq. (8) has a small effect on the cell power P (see Fig. 6). Namely, if the phonon occupation number n_v is large then decoherence due to stimulated phonon emission will dominate the other environmental decoherence channels (τ_2 effects). As a result, one can have a cell in which τ_2 does not affect the cell power until $\gamma_\tau \equiv 1/\tau_2$ becomes comparable with $n_v(\tilde{\gamma}_1 + \tilde{\gamma}_2) \gg \tilde{\gamma}_1 + \tilde{\gamma}_2$. As an illustration we consider a model in which levels b_1 and b_2 are degenerate and take $T_S = 0.5$ eV, $T_a = 0.0259$ eV, $E_a - E_b = 1.43$ eV (GaAs band-gap), $E_a - E_c = E_v - E_b = 0.0002$ eV, $E_c - E_v = 1.4296$ eV, $\gamma_2 = 0.01\gamma_1$, $\tilde{\gamma}_1 = 50\gamma_1$, $\tilde{\gamma}_2 = 10^{-5}\gamma_1$ and $\tilde{\Gamma} = 50\gamma_1$. Fig. 6 shows, that for such parameters, Fano interference is robust against the environmental decoherence.

Summary and Discussion. One can understand the Fano enhancement for the photocell of Fig. 1 as follows. Suppose a solar photon tuned to the band edge is absorbed and an electron is promoted from the valence state $|b\rangle$ to the conduction states $|a_1\rangle$ and $|a_2\rangle$. Then the electron may proceed to the conduction reservoir state $|c\rangle$ and produce useful work by passing through a load and returning to state $|b\rangle$ via $|v\rangle$. On the other hand the electron may fall back to $|b\rangle$ via stimulated or spontaneous emission of a solar photon of energy E_{ab}. We would like to minimize this radiative recombination process and this is what Fano interference allows us to do by increasing the current through the photovoltaic cell via quantum coherence.

For the scheme of Fig. 3 the Fano interference enhances absorption of solar photons. Namely, the $\tilde{\gamma}_{12}$-terms result in redistribution of the population between $|b_1\rangle$ and $|b_2\rangle$ states such that the state with stronger coupling to the upper level $|a\rangle$ becomes more populated. This increases the number of absorbed photons and the current through the cell (dash line in Fig. 4). The γ_{12}-terms yield interference between the photon absorption channels $b_1 \to a$ and $b_2 \to a$. Such interference can enhance photon absorption as in the present model or suppress it which is the case for lasing without inversion [1].

This is essentially different from the quantum coherence produced by an external microwave field, which, as discussed in [3], costs energy. The extra energy supplied by microwaves can yield an open circuit voltage exceeding the energy of the solar photon. Moreover, using phase coherent atoms one can make a device that can even oper-

ate by extracting energy from a single thermal reservoir. One such scheme is the photo-Carnot engine in which a beam of atoms was used to drive a single mode of the radiation field; which in turn was the working fluid which exerted pressure on the piston [2]. In particular, a very tiny amount of quantum coherence can lead to a substantial few percent increase in efficiency. But this does not violate thermodynamics since preparation of coherent atoms costs energy which is supplied by an external source [15]. In any case a perpetual motion machine of the second kind is never suggested or implied.

In the present paper, quantum coherence is generated by the photocurrent due to Fano interference. No additional energy source is necessary to create such induced coherence. Nevertheless, as we have shown, the induced coherence can, in principle, enhance power (current) of photovoltaic devices such as solar cells and/or photodetectors. Furthermore, proper selection of photocell parameters can reduce the effect of decoherence τ_2 on Fano power enhancement.

We gratefully acknowledge support of the National Science Foundation Grant EEC-0540832 (MIRTHE ERC), the Office of Naval Research and the Robert A. Welch Foundation (Award A-1261).

[1] For a review see O. Kocharovskaya, Phys. Rep. **219**, 175 (1992); S. Harris, Phys. Today **50**, 36 (1997); M.O. Scully and M.S. Zubairy, Quantum Optics (Cambridge University Press, Cambridge, UK, 1997).

[2] The quantum photon engine is treated in M. Scully, S. Zubairy, G. Agarwal, and H. Walther, Science **299**, 862 (2003). The classical photon heat engine is nicely discussed in M. H. Lee, Am. J. Phys. **69**, 874 (2001).

[3] M. Scully, Phys. Rev. Lett. **104**, 207701 (2010).

[4] Another interesting connection can be made with the quantum efficiency of the laser without inversion as discussed in M. Scully, Phys. Rev. Lett. **106**, 049801 (2011); arXiv:1012.5321v2 [quant-ph].

[5] Ref. [3] focuses on enhancing the quantum efficiency via radiatively induced quantum coherence. As we show here, Fano induced coherence can yield an essentially equivalent result enhancing the cell power.

[6] A. Kirk, Phys. Rev. Lett. **106**, 048703 (2011).

[7] Specifically, Kirk states in [6] that: "As Harris shows . . . Fano interference does not break detailed balance." We disagree with this statement; as does Harris, and we thank him for allowing us to so report.

[8] S. Harris, Phys. Rev. Lett. **62**, 1033 (1989).

[9] M. Fleischhauer, T. McIllrath and M. O. Scully, Appl. Phys. B **60**, 123 (1995); M. Fleischhauer et. al., Opt. Commun. **94**, 599 (1992).

[10] G. Agarwal, *Quantum Statistical Theories of Spontaneous Emissions and Their Relation to other Approaches*, Springer Tracts in Modern Physics Vol. 70 (Springer, Berlin, 1974).

[11] W. Schleich, *Quantum Optics in Phase Space*, (Wiley-VCH, 2002).

[12] A. Nozik, Physica (Amsterdam) **14E**, 115 (2002).

[13] V. Kozlov, Yu. Rostovtsev and M. Scully, Phys. Rev. A **74**, 063829 (2006). The Agarwal-Fano process of the present paper, is modeling a quantum dot solar cell placed in a hohlraum which is driven by narrow band isotropic radiation. However, one can extend the present analysis to the case of directional incident solar radiation and isotropic spontaneous emission.

[14] A. Rose, J. Appl. Phys. **31**, 1640 (1960).

[15] The discussion of the photo-Carnot engine given in [3] is rejected by Kirk [6] who incorrectly says that "phaseonium" is a working fluid. We want to emphasize that photons are the working fluid in the photo-Carnot engine, just as steam is the working fluid in a steam engine. Phaseonium is the fuel, analogous to coal in a steam engine.